Heliyon 10 (2024) e31686

Contents lists available at ScienceDirect

Heliyon

journal homepage: www.cell.com/heliyon

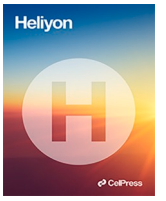

Research article

Virtual parameter calibration of pod pepper seeds based on discrete element simulation

Xingye Chen, Xinzhong Wang *, Jing Bai, Weiquan Fang, Tianyu Hong, Nan Zang, Gaoliang Wang

School of Agricultural Engineering, Jiangsu University, Zhenjiang, 212013, China

ARTICLE INFO

Keywords:
Pod pepper seeds
Discrete element method
Angle of repose
Response surface methodology
Contact parameter

ABSTRACT

In order to achieve numerical optimization of the pod pepper seed sowing device, the contact parameters of pod pepper seeds were calibrated, with the angle of repose used as the response value. A set of discrete element method (DEM) models of pod pepper seeds was developed to simulate the formation of seed repose angles using reverse engineering reconstruction techniques. An eight-factor, three-level response surface experiment based on the Box-Behnken central combination test method was performed to study the effects of various factors on the angle of repose of seeds. The angle of repose obtained from physical experiments with a value of 27.56° was taken as the target value. The optimal combination of parameters is obtained as follows: seed Poisson's ratio of 0.22, seed shear modulus of 15.47 MPa, seed-to-seed static friction coefficient of 0.25, seed-to-seed rolling friction coefficient of 0.67, seed-to-seed collision recovery coefficient of 0.64, seed-to-steel-plate static friction coefficient of 0.55, seed-to-steel-plate rolling friction coefficient of 0.45, and seed-to-steel plate collision recovery coefficient of 0.34. A two-sample *t*-test of the angle of repose obtained by the cylinder lifting method and the pumping plate method against the target value yielded $P > 0.05$, indicating the reliability of the simulation experiments.

1. Introduction

Pod pepper is a kind of dried chili pepper grown in large quantities in mainland China that is highly favored by consumers as a vegetable and a condiment [1]. The planting of pod pepper is crucial to its production process, and mechanized seeding is the main way to increase the planting efficiency. Seed dispensers play a pivotal role in the seeding process [2]. Scholars at home and abroad also have conducted a lot of research on the seed discharging device in order to improve its working performance [3–5]. In recent years, with the development of computer technology, the discrete element method (DEM) has been extensively applied in agricultural equipment research [6–8]. Studying the interaction between the key components of seed dischargers and seeds through the discrete element method may provide, a reference basis for their design and optimization, which can effectively improve research and development efficiency and reduce the required costs.

Currently, researchers both domestically and internationally have calibrated discrete element model simulation parameters for corn, soybeans, potatoes, pellet feed, and other agricultural products. Guo et al. established a mechanical model of banana stalks and investigated their biomechanical properties by combining physical and simulation tests [9]. Peng et al. measured the angle of repose of

* Corresponding author.
E-mail address: xzwang@ujs.edu.cn (X. Wang).

https://doi.org/10.1016/j.heliyon.2024.e31686
Received 1 March 2024; Received in revised form 20 May 2024; Accepted 20 May 2024
Available online 21 May 2024

pellet feeds through the injected cross-section method and obtained the optimal simulation parameter combinations for large pig feeds using the response surface method [10]. Zhang et al. carried out real tests and simulation measurements of bottomless cylinder lifting and slip stacking to calibrate the interspecies static and rolling friction factors of seed models with different radii of filled ball particles using the surface response method with angle of repose as an indicator [11]. Coetzee et al. determined the particle stiffness by compression tests and calibrated the friction coefficients of the particles by angle of repose tests, thus greatly simplifying the DEM modeling process for large particle systems [12]. Lee and Park. designed four simulated friction tests to determine the static and rolling friction coefficients between materials and materials, and between materials and containers, and to check the accuracy of the measured coefficients by using the angle of repose as the target value [13]. Ghodki et al. calibrated the DEM input parameters of the soybean Hertz-Mindlin model by comparing experimental and numerical simulation results by employing a self-made box device, which contributed to the implementation of subsequent simulation tests of soybean harvesting machinery [14]. Wang et al. defined two contact materials for corn seed angle of repose simulation tests to achieve the contact parameters of corn seed using the actual measured angle of repose as the optimal target value [15]. Liu et al. calibrated and aligned the discrete element simulation parameters of miniature potatoes on the basis of a combination of experimental measurements and simulation tests [16]. With the aid of EDEM discrete element simulation software, Zhang et al. selected the Hertz-Mindlin bonding model to construct a mung bean seed particle model, calibrated the contact parameters of mung bean seeds, and processed and optimized the data by taking the relative error between the simulation repose angle and the actual repose angle as an index [17]. In summary, in the current research for discrete element simulation parameter calibration, most of the calibration objects are mostly large seeds, fruit, potatoes, and other materials, and there are relatively few studies on determining and calibrating the simulation parameters of vegetable seeds, such as pod pepper seeds.

In this paper, a combination of physical and simulation tests was used to study the physical and contact parameters of pod pepper seeds, and the measured values of physical tests and the existing data from domestic and international literature were leveraged as the basis for the selection of the simulation parameter ranges. An eight-factor, three-level quadratic regression response surface test with seed repose angle as the response value was conducted to calibrate and benchmark the discrete meta-simulation parameters of pod pepper seeds. Through the simulation of angle of repose regression modeling and significance tests, the reasonableness of the experiment was verified, and the influence of each factor on the angle of repose was analyzed, with the parameters that caused the most significant effect on the angle of repose screened out simultaneously. Additionally, the surface analysis of the simulated angle of repose of and related parameters was carried out to analyze its changing trend. Finally, two kinds of simulation experiments, based on the cylinder lifting method and the pumping plate method, were combined with physical experiments for T detection to validate and determine the reliability of the simulation experiments, and to obtain the optimal combination of simulation parameters, with a view to providing a reference for the discrete meta-simulation of other irregular materials with small particles.

2. Materials and methods

2.1. Geometric modeling of pod pepper seeds

The pod pepper seeds used in this paper which were full and free of impurities were purchased from Anhui Jintai Seed Industry Company Limited. 200 seeds of pod pepper were randomly selected, and then, categorized as flat, with little obvious thickness changes, and a concave-convex shape presented on the two sides and middle of the seeds, according to the morphological characteristics of seed thickness differences, as shown in Fig. 1 (a). The three-dimensional dimensions of the seeds ($L \times W \times T$) were measured using a vernier caliper with an accuracy of 0.02 mm, as shown in Fig. 1(b). The range of values of length L, width W, and thickness T and the quantity statistics of 200 seeds of pod pepper are displayed in Table 1.

2.2. Determination of seed density and water content of pod pepper seeds

1,000 seeds of pod pepper were randomly selected and the seed mass of 1,000 grains was measured with an electronic weighing scale with an accuracy of 0.01 g. The experiment was repeated five times, and the average value of the results (5.4 g) was taken as the

Fig. 1. Pod pepper seed sample (a) morphology classification (b) dimension parameters.

Table 1
Pod pepper seed size statistics.

Items	Proportion (%)	Quantity	L (mm)	W (mm)	T (mm)
Flat seeds	70.5	35	4.30–4.50	3.25–3.35	1.05–1.10
		35	4.10–4.30	3.15–3.25	1.00–1.05
		36	3.90–4.10	3.05–3.15	0.95–1.00
		35	3.70–3.90	2.95–3.05	0.90–0.95
Concave-convex seeds	29.5	20	4.20–4.40	3.00–3.10	1.15–1.20
		20	4.00–4.20	2.90–3.00	1.10–1.15
		19	3.80–4.00	2.80–2.90	1.05–1.10

mass of the pod pepper seeds. The drainage method was used to measure the volume of 1000 seeds of pod pepper, and the average value was 5.74 cm^3 for 5 repetitions. The density of pod pepper seeds was 0.94 $g \cdot cm^{-3}$ calculated by Equation (1).

$$\rho = \frac{m}{v} \tag{1}$$

where, ρ is the density of the measured material, ($g \bullet cm^{-3}$); m refers to the mass of the measured material, (g); v means the volume of the measured material, (cm^3).

50 g of pod pepper seeds was randomly chosen, and evenly divided into 5 parts. Subsequently, the seeds were dried in a B0D-75-II type electric thermostatic drying oven, and weighed again after cooling to room temperature. According to Equation (2), the average moisture content of pod pepper seeds was calculated as 6.43 %.

$$M_d = \frac{m_w}{m_s} \tag{2}$$

where, M_d is the dry basis moisture content, (%); m_w is the mass of water contained in the material, (g); m_s is the mass of dry matter contained in the material, (g).

2.3. Establishment of a three-dimensional model of pod pepper seeds

The shape of the simulation model has a great influence on the calibration results of contact parameters [18]. The more similar the three-dimensional model of pod pepper seeds is to the real shape, the more accurate the simulation results will be. As can be seen from Fig. 1 and Table 1, the shape of pod pepper seeds was very complex, and the size and shape of pod pepper seeds varied greatly. Generally, it is not possible to build a single model to represent the whole sample of pod pepper seeds by direct modeling. Therefore, as shown in Fig. 2(a), seven samples of the same-sized seeds (four flattened and three concave-convex) of pod pepper were selected on the basis of the morphology, proportions, and mean sizes of pod pepper seeds. A hand-held blue laser 3D scanner (measuring rate up to 480,000 measurements·s^{-1}, resolution up to 0.01 mm, 14 blue laser lines + 1 scanning beam for deep holes + 5 scanning lines for details), model Rigel Scan Elite, was adopted to scan the peripheral contours of the seeds of pod pepper. In order to obtain a well-represented set of three-dimensional models of pod pepper seeds, the scanned point cloud data were imported into Geomagic Studio (2013, Geomagic, Inc.) software for fitting [19], as shown in Fig. 2(b).

2.4. Shear modulus and Poisson's ratio of pod pepper seeds

Shear modulus (G) is an elastic parameter that characterizes the stiffness of a particle. The shear modulus of elastic, homogeneous, and isotropic materials is related to Poisson's ratio (σ) and elastic modulus (E), as shown in Equation (3) [20].

$$G = \frac{E}{2(1+\sigma)} \tag{3}$$

Combining literature on agricultural materials such as flaxed seeds [21], agropyron seeds [22], oil sunflower seeds [23], wheat

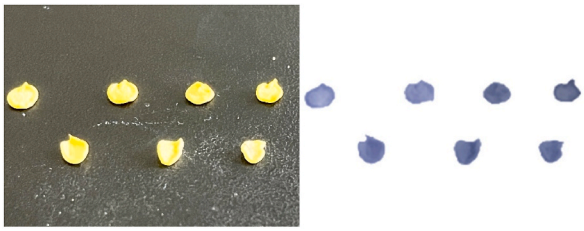

(a) (b)

Fig. 2. -Three-dimensional modeling of pod pepper seeds (a) Prototype of pod pepper seeds (b) Corresponding 3D model.

[24], brown rice [25], and mung beans [17], the maximum and minimum shear modulus values of pod pepper seeds were identified in this paper, with an appropriate range of expansion, by taking 200 MPa as the upper limit and 4 MPa as the lower limit of shear modulus. Considering that the Poisson's ratio of agricultural materials is in the range of 0.2–0.4 [26–28], a similar range was chosen for calibration of pod pepper seeds in this paper.

2.5. Determination of contact parameters in the seeds of pod pepper

2.5.1. Determination of static friction coefficient

The coefficient of static friction is the ratio of the friction force to the normal force acting between two contact surfaces. The coefficient of static friction between particles and particles, and between particles and walls, is required to carry out the parameter calibration of pod pepper seeds. In this paper, the coefficient of static friction between different materials was measured using the oblique method [23]. The test material was a 500 mm × 150 mm × 3 mm steel plate beveled, as shown in Fig. 3. To start the test, a steel ramp was first placed on a horizontal table. Then, the seeds were placed on the ramp, and one end of the ramp was slowly raised. When the measured material exhibited a tendency to slide, the inclined plane stopped lifting, and the angle between the inclined plane and the horizontal tabletop was recorded at this time. The test was repeated for 10 times. Through Equation (4), the coefficient of static friction between the pod pepper seeds and the steel plate was calculated as 0.43.

$$\gamma = \frac{f}{F} = \frac{G \sin \alpha}{G \cos \alpha} = \tan \alpha \tag{4}$$

where, α is the angle between the inclined plane and the horizontal plane, (°); γ is the coefficient of static friction between the pod pepper seeds and the steel plate; f indicates the friction between the seeds of the pod pepper and the steel plate, (N); F is the support force of the steel plate on the seeds of the pod pepper, (N); and G represents the gravitational force exerted on the seeds of pod pepper, (N).

The limiting values of static friction for agricultural products are considered to be 0.2 and 0.6. The coefficients of static friction between fava bean and red clover seeds, which are similar in shape to pod pepper seeds, and steel plates are 0.457 [29] and 0.38 [30], respectively. The particle-particle static friction values are similar, as the coefficients of static friction between seeds of seeded melons and between radix peucedani seeds are 0.25 [31] and 0.53 [32], respectively. Therefore, the limiting values of static friction coefficients of seed-to-seed and seed-to-steel plates were taken as 0.2 and 0.6 in this paper.

Note: α is the angle between the slope of the steel plate and the horizontal ground, (°); F is the support force of steel plate to pod pepper seeds, (N); f is friction force, (N); G is the gravity of pod pepper seeds, (N).

2.5.2. Determination of rolling friction coefficient

The rolling friction coefficient is the ratio of the friction force to the friction of the normal force preventing the particles from rolling. In DEM modeling, the shape of non-spherical particles is usually represented by an arbitrary increase in the rolling friction coefficient [33]. In this paper, the rolling friction coefficients between agricultural materials similar in shape to pod pepper seeds, and between agricultural materials and steel plates were investigated. According to relevant literature, the coefficient of rolling friction between seed melon seeds is 0.25, and that between seed melon seeds and steel plate is 0.75 [31]. The coefficient of rolling friction between chili pepper seeds is 0.75 and that between chili pepper seeds and steel plate is 0.60 [34]. In this study, by extending the value range appropriately, the range of values for the coefficients of rolling friction between pod pepper seeds and between the seeds and the steel plate was determined to be 0.10–0.90.

2.5.3. Determination of the collision recovery coefficient

The collision recovery coefficient is an important parameter in bulk analysis and is a measure of the ability of an object to return to

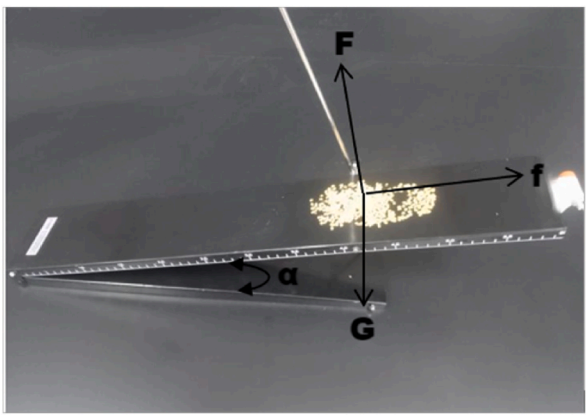

Fig. 3. Measurement test of coefficient of static friction of pod pepper seeds.

its original shape after a collision [21]. A review of national and international literature shows that the values of the collision recovery coefficients between agricultural material species such as rapeseed [35], wheat [36], and soybeans [37,38] range from 0.1 to 0.7, and those with steel plates range from 0.4 to 0.7. Therefore, the range of particle-particle and particle-wall contacts, including published data, was taken as 0.1–0.7 in this research.

2.6. Determination of the repose angle of pod pepper seeds

As shown in Fig. 4, the cylinder lifting method was used to obtain the pod pepper seed pile to measure the angle of repose [39,40]. During the test, a bottomless steel cylinder with an inner diameter of 50 mm and a height of 200 mm was placed squarely on a horizontal table, to make its bottom surface in contact with the table. Afterwards, 2000 pod pepper seeds were injected into the cylinder, and then the cylinder was slowly lift upwards at a speed of 0.05 m • s^{-1} until the pod pepper seeds changed to a stable pile of material on the table. The angle of repose of the pod pepper seeds at this time was measured.

As shown in Fig. 5, images of stacked pod pepper seeds were processed using MATLAB (R2018b, Mathematical Engineering, Inc.) image processing techniques. After grayscale processing, binarization, contour extraction, and line fitting, the mean value of the angle of repose of both left and right sides of the pod pepper seeds was determined to be 27.56°.

2.7. Simulation of DEM model of pod pepper seeds

The ranges of basic physical property parameters of pod pepper seeds and steel plates were obtained through several pre-simulation tests and in conjunction with relevant literature [26,41], as shown in Table 2. The previously established three-dimensional model group of pod pepper seeds was imported into the discrete element simulation software EDEM 2022 in stl format as a particle template. Subsequently, the particle template of pod pepper seeds was filled by single spherical particles in the software to establish the discrete element simulation model of pod pepper seeds (7 species in total), as shown in Fig. 6.

As shown in Fig. 7(a), in the first stage, a virtual cylinder with a diameter of 50 mm was created by the EDEM software at the upper aperture of a bottomless cylinder with an inner diameter of 50 mm and a height of 200 mm, which was used as a particle factory to generate pod pepper seed particles. The particles were generated dynamically, with an initial velocity of 0.1 m • s^{-1} in the -Z direction. A total of 2000 seeds were produced based on the proportions of the seven pod pepper seed models in Table 1, with gravitational acceleration of 9.81 m • s^{-2}, a generation rate of 1000 *Pieces* • s^{-1}, the production time of 2 s, and a time step of 3×10^{-6}s. The mesh size was 6 times the radius of the smallest particle, and Hertz-Mindlin was chosen as the simulation contact model (no slip). As shown in Fig. 7(b), in the second stage, an upward lifting velocity of 0.05 m • s^{-1} was applied to the cylinder. After 4s of simulation time, a stable pile of pod pepper seed particles was finally created on the bottom plate, and the simulation angle of repose was measured using the protractor function that comes with the EDEM software.

The basic parameters required for the simulation of discrete elemental particle stacking of pod pepper seeds included the intrinsic parameters of pod pepper seeds, the material properties of the contact materials, and the range of values of the relevant parameters determined from the previous experiments as well as the relevant information, as shown in Table 2.

3. Result and discussion

3.1. Box-Behnken experimental design

The design of the Box-Behnken test was performed with the assistance of Design-Expert (13.0.1.0, Stat-Ease, Inc.) software. In order to increase the accuracy of the simulation experiment, Box-Behnken central combination experimental design theory was selected to carry out an eight-factor, three-level quadratic regression response surface test with 120 groups [42–45]. The maximum and minimum values of the eight test parameters in Table 2 were coded as levels +1 and −1, respectively, to obtain a table of test factor levels as

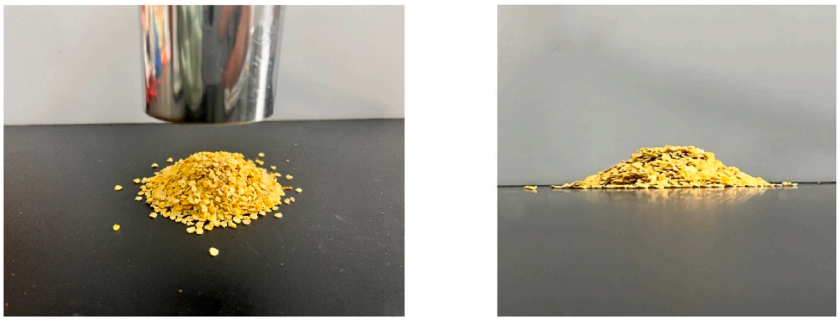

(a) (b)

Fig. 4. Cylinder lifting method to measure the angle of repose of pod pepper seeds (a) Cylinder lifting process diagram (b) Side view of pod pepper seed pile.

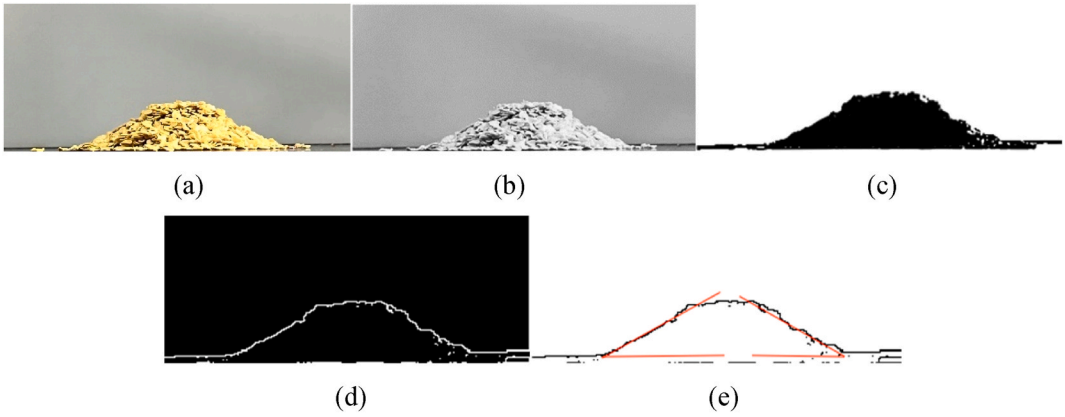

Fig. 5. Measurement of the angle of repose of pod pepper seeds using MATLAB (a) Original photograph; (b) Grayscale processing; (c) Binarization; (d) Contour extraction; (e) Line fitting.

Table 2
Range of simulation parameters.

Parameter	Symbol	Base value	Range
Density of pod pepper seed (g • cm^{-3})	ρ_p	0.94	
Poisson's ratio of pod pepper seed	v_p	0.3	0.2–0.4
Shear modulus of pod pepper seed (MPa)	G_p	102	4–200
Coefficient of static friction between pod pepper seed and pod pepper seed	$\mu_{s\ pp}$	0.4	0.2–0.6
Coefficient of static friction between pod pepper seed and steel plate	$\mu_{s\ ps}$	0.4	0.2–0.6
Coefficient of rolling friction between pod pepper seed and pod pepper seed	$\mu_{r\ pp}$	0.5	0.1–0.9
Coefficient of rolling friction between pod pepper seed and steel plate	$\mu_{r\ ps}$	0.5	0.1–0.9
Collision recovery coefficient between pod pepper seed and pod pepper seed	C_p	0.4	0.1–0.7
Collision recovery coefficient between pod pepper seed and steel plate	C_s	0.4	0.1–0.7
Density of Steel Plate (g • cm^{-3})	ρ_s	7.85	
Poisson's ratio of Steel Plate	v_s	0.30	
Shear modulus of Steel Plate (MPa)	G_s	8×10^4	

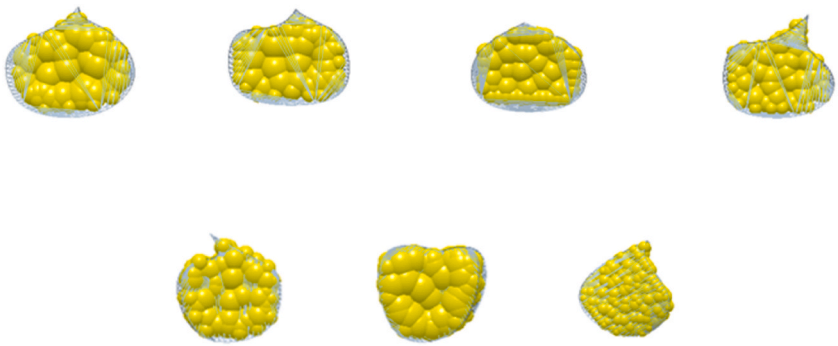

Fig. 6. -Three-dimensional model of pod pepper seeds.

shown in Table 3.

3.2. Test results and analysis

The Box-Behnken test design scheme and results are displayed in Table 4, where the factor combinations were ranked, encompassing seed Poisson's ratio (v_p), seed shear modulus (G_p), coefficient of static friction between seed and seed ($\mu_{s\ pp}$), coefficient of rolling friction between seed and seed ($\mu_{r\ pp}$), coefficient of recovery from collision of seed with seed (C_p), coefficient of static friction between seed and steel plate ($\mu_{s\ ps}$), coefficient of rolling friction between seed and plate ($\mu_{r\ ps}$), and coefficient of recovery from collision of seed and plate (C_s).

(a) (b)

Fig. 7. Simulation test of repose angle (a) Filling the cylinder with 2000 seed pellets (b) Lift the cylinder.

Table 3
Table of factors and levels.

Codes	v_p	G_p	$\mu_{s\ pp}$	$\mu_{r\ pp}$	C_p	$\mu_{s\ ps}$	$\mu_{r\ ps}$	C_s
−1	0.2	4	0.2	0.1	0.1	0.2	0.1	0.1
0	0.3	102	0.4	0.5	0.4	0.4	0.5	0.4
1	0.4	200	0.6	0.9	0.7	0.6	0.9	0.7

3.3. Simulated repose angle regression modeling and significance test

Based on the experimental results in Table 4, the simulated angle of repose was analyzed by ANOVA through the Box-Behnken test, and the results of excluding the terms with F less than 1 are organized in Table 5. A *P*-value was used to analyze the significance of the object, with $P < 0.01$ representing that the response model was highly significant, and $P < 0.05$ suggesting that the response model was significant. The regression equation for the angle of repose of the simulation was obtained as:

$$\theta = 27.63 + 0.06v_p + 1.01\mu_{s\ pp} + 1.02\mu_{r\ pp} + 0.49\mu_{s\ ps} + 0.52\mu_{r\ ps} - 0.07v_p\mu_{r\ ps} + 0.07\mu_{r\ pp}\ C_p + 0.07\mu_{r\ pp}\ \mu_{s\ ps} - 0.06\mu_{s\ pp}^2 \tag{5}$$

As shown in Table 5, when the *P*-value of the regression model was less than 0.01, it meant that the established regression model was highly significant, and when the misfit term of the model was 0.2258, greater than 0.05, indicating that the model was well fitted and no misfit occurred. The coefficient of determination of the model, $R^2 = 0.9895$, changed to $R^2 = 0.9833$ after adjustment, which was very close to 1. Moreover, the coefficient of variation, CV = 0.5183 %, and the precision, Adeq Precision = 58.9022, revealed that the regression model was significantly reliable and could be adopted for further prediction analysis of target angle of repose.

In this regression model, the *P*-values of the v_p、 $\mu_{s\ pp}$、 $\mu_{r\ pp}$、 $\mu_{s\ ps}$、 $\mu_{r\ ps}$ terms were less than 0.01, which indicated that they were within the 99 % confidence interval with an extremely significant effect on the regression model. The *P*-values of the $v_p\mu_{r\ ps}$、 $\mu_{r\ pp}C_p$、 $\mu_{r\ pp}\mu_{s\ ps}$、 $\mu_{s\ pp}^2$ terms are less than 0.05, indicating that the effect on the regression model was significant.

3.4. Analysis of the effect of each factor on the influence of the simulation repose angle

According to the F-value results in Table 5, the degree of influence of individual factors on the simulated angle of repose regression model of pod pepper seeds could be measured, which was reflected by the contribution value K. It presented a positive correlation, that is, the larger the K value, the greater the degree of influence [46].

The formula for calculating the K value is as follows:

$$\delta = \begin{cases} 0 & F \le 1 \\ 1-\dfrac{1}{F} & F > 1 \end{cases} \tag{6}$$

$$K_{Xj} = \delta_{Xj} + \frac{1}{2}\sum \delta_{XiXj} + \delta_{Xj}^2 \tag{7}$$

where, F is the F-value of the analysis of variance and δ is the appraisal value. The contribution of each factor to the simulated angle of repose was calculated according to equations (6) and (7), and the results are displayed in Table 6.

Table 4
Box-Behnken experiment design scheme and results.

Test No.	v_p	G_p	$\mu_{s\ pp}$	$\mu_{r\ pp}$	C_p	$\mu_{s\ ps}$	$\mu_{r\ ps}$	C_s	Simulated angle of repose $\theta^{'}$/(°)
1	1	0	0	−1	0	1	−1	0	26.71
2	1	0	1	0	0	−1	0	−1	28.15
3	0	−1	0	1	−1	0	1	0	29.02
4	0	−1	0	−1	0	1	0	1	27.13
5	0	0	0	0	1	1	−1	−1	27.61
6	0	0	−1	1	1	−1	0	0	27.15
7	0	−1	1	0	0	1	−1	0	28.60
8	0	−1	0	1	1	0	−1	0	28.06
9	0	0	0	0	0	0	0	0	27.55
10	−1	−1	0	0	1	1	0	0	28.11
11	1	0	0	−1	1	0	0	−1	26.59
12	−1	1	1	−1	0	0	0	0	27.64
13	0	0	−1	−1	0	0	−1	−1	25.05
14	0	−1	0	−1	0	−1	0	−1	26.14
15	1	0	0	1	0	1	1	0	29.62
16	0	1	0	−1	0	1	0	−1	27.11
17	−1	0	1	0	0	−1	0	1	28.14
18	−1	0	−1	0	−1	0	−1	0	26.07
19	0	0	0	0	−1	1	−1	1	27.54
20	1	1	0	0	0	0	−1	−1	27.08
21	−1	−1	0	0	0	0	1	1	28.32
22	−1	0	1	0	−1	0	1	0	29.09
23	0	1	1	0	0	1	1	0	29.59
24	−1	0	0	1	0	1	−1	0	28.59
25	0	0	−1	1	0	0	1	−1	28.12
26	−1	−1	0	0	−1	−1	0	0	27.01
27	0	0	0	0	0	0	0	0	27.62
28	1	1	0	0	−1	−1	0	0	27.16
29	1	0	1	0	0	1	0	1	29.11
30	1	0	0	1	−1	0	0	−1	28.48
31	0	−1	0	−1	−1	0	−1	0	26.04
32	0	0	0	0	−1	−1	−1	−1	26.44
33	0	0	1	−1	0	0	−1	1	27.14
34	−1	−1	0	0	0	0	−1	−1	27.01
35	0	−1	1	0	0	−1	1	0	28.49
36	1	0	−1	0	−1	0	1	0	27.17
37	1	1	1	1	0	0	0	0	29.84
38	−1	0	−1	0	0	1	0	1	27.11
39	−1	1	0	0	0	0	1	−1	28.06
40	0	0	0	0	0	0	0	0	27.60
41	0	0	0	0	0	0	0	0	27.57
42	−1	0	0	−1	−1	0	0	−1	26.41
43	0	−1	0	−1	1	0	1	0	27.11
44	−1	1	0	0	1	−1	0	0	27.15
45	0	0	−1	1	0	0	−1	1	27.04
46	0	1	0	1	−1	0	−1	0	28.09
47	0	0	1	−1	0	0	1	−1	27.99
48	0	1	−1	0	1	0	0	−1	26.58
49	0	1	−1	0	0	−1	1	0	26.43
50	−1	0	1	0	0	1	0	−1	29.03
51	0	0	−1	−1	1	1	0	0	25.21
52	0	0	1	1	−1	−1	0	0	29.01
53	−1	0	0	−1	1	0	0	1	26.65
54	1	0	0	1	1	0	0	1	28.76
55	1	0	0	−1	−1	0	0	1	26.71
56	−1	1	0	0	−1	1	0	0	28.10
57	0	0	0	0	1	1	1	1	28.71
58	0	0	1	1	0	0	−1	−1	29.05
59	0	−1	0	1	0	1	0	−1	28.99
60	0	0	0	0	−1	1	1	−1	28.51
61	1	1	−1	−1	0	0	0	0	25.67
62	0	−1	−1	0	−1	0	0	−1	26.44
63	0	0	0	0	−1	−1	1	1	27.53
64	1	−1	0	0	−1	1	0	0	28.07
65	1	0	−1	0	0	−1	0	1	26.19
66	0	1	0	1	0	−1	0	−1	28.10
67	0	1	1	0	1	0	0	1	28.54
68	1	−1	0	0	1	−1	0	0	27.08

(*continued on next page*)

Table 4 (*continued*)

Test No.	v_p	G_p	$\mu_{s\ pp}$	$\mu_{r\ pp}$	C_p	$\mu_{s\ ps}$	$\mu_{r\ ps}$	C_s	Simulated angle of repose $\theta^{'}$/(°)
69	0	−1	−1	0	0	−1	−1	0	25.45
70	−1	0	−1	0	0	−1	0	−1	26.01
71	0	1	1	0	0	−1	−1	0	27.61
72	1	1	0	0	0	0	1	1	28.14
73	1	0	0	−1	0	−1	1	0	26.61
74	0	0	−1	−1	−1	−1	0	0	25.06
75	0	1	0	−1	1	0	−1	0	26.08
76	−1	0	1	0	1	0	−1	0	27.05
77	0	−1	−1	0	1	0	0	1	26.51
78	0	0	−1	−1	0	0	1	1	26.03
79	−1	0	0	1	1	0	0	−1	28.59
80	0	1	0	−1	−1	0	1	0	27.08
81	−1	−1	1	1	0	0	0	0	29.45
82	−1	0	0	1	0	−1	1	0	28.51
83	1	−1	0	0	0	0	−1	1	27.23
84	0	1	0	1	0	1	0	1	29.02
85	0	1	1	0	−1	0	0	−1	28.64
86	0	1	0	1	1	0	1	0	29.19
87	0	0	0	0	0	0	0	0	27.57
88	0	0	1	−1	1	−1	0	0	27.08
89	0	0	0	0	0	0	0	0	27.70
90	1	−1	−1	1	0	0	0	0	27.65
91	0	0	0	0	1	−1	−1	1	26.63
92	−1	0	0	−1	0	1	1	0	27.52
93	−1	0	0	−1	0	−1	−1	0	25.44
94	−1	0	0	1	−1	0	0	1	28.50
95	1	1	0	0	1	1	0	0	28.20
96	0	−1	1	0	1	0	0	−1	28.51
97	−1	0	−1	0	1	0	1	0	27.00
98	−1	1	−1	1	0	0	0	0	27.60
99	0	0	1	−1	−1	1	0	0	28.04
100	0	0	1	1	0	0	1	1	30.14
101	0	−1	0	1	0	−1	0	1	28.08
102	0	1	−1	0	0	1	−1	0	26.63
103	0	0	−1	1	−1	1	0	0	28.09
104	0	1	−1	0	−1	0	0	1	26.58
105	1	0	1	0	−1	0	−1	0	28.14
106	1	0	1	0	1	0	1	0	29.22
107	−1	1	0	0	0	0	−1	1	27.24
108	1	0	−1	0	0	1	0	−1	27.13
109	1	0	−1	0	1	0	−1	0	26.31
110	0	1	0	−1	0	−1	0	1	26.30
111	1	−1	0	0	0	0	1	−1	28.15
112	0	−1	−1	0	0	1	1	0	27.61
113	1	0	0	1	0	−1	−1	0	27.63
114	0	−1	1	0	−1	0	0	1	28.61
115	0	0	1	1	1	1	0	0	30.14
116	−1	−1	−1	−1	0	0	0	0	25.41
117	0	0	0	0	0	0	0	0	27.57
118	0	0	0	0	1	−1	1	−1	27.65
119	1	−1	1	−1	0	0	0	0	27.63
120	0	0	0	0	0	0	0	0	27.88

3.5. Simulation of the angle of repose with corresponding surface analysis of relevant parameters

According to Table 6, three factors that had large effects on the angle of repose of pod pepper seeds were screened out: seed-to-seed static friction coefficient ($\mu_{s\ pp}$), seed-to-seed rolling friction coefficient ($\mu_{r\ pp}$), and seed-to-steel plate rolling friction coefficient ($\mu_{r\ ps}$), and their interactions were analyzed as shown in Fig. 8. As observed from Fig. 8(a), the angle of repose of seeds reached its maximum value when the coefficient of static friction between seed and seed ($\mu_{s\ pp}$) and the coefficient of rolling friction between seed and seed ($\mu_{s\ pp}$) of pod pepper were both at high levels. According to Fig. 8(b), when the coefficient of static friction between seed and seed ($\mu_{s\ pp}$) or the coefficient of rolling friction between seed and steel plate ($\mu_{r\ ps}$) of pod pepper was certain, the angle of repose of the seed increased linearly with the increase of the coefficients of static and rolling friction, and the coefficient of static friction between seed and seed ($\mu_{s\ pp}$) caused a greater effect on the angle of repose than the coefficient of rolling friction between seed and steel plate ($\mu_{r\ ps}$). As can be seen from Fig. 8(c), when the coefficient of seed-to-seed rolling friction ($\mu_{r\ pp}$) was certain, the angle of repose increased slowly with the increase in the coefficient of seed-to-steel plate rolling friction ($\mu_{r\ ps}$), and when the coefficient of seed-to-steel plate rolling friction ($\mu_{r\ ps}$) was certain, the angle of repose demonstrated a larger increase with the increase in the coefficient of seed-to-seed

Table 5
Variation analysis of Box-Behnken quadratic model.

Source of variance	Sum of square	Degree of freedom	Mean square	F-value	*P*-value
Model	144.47	44	3.28	160.71	<0.01
v_p	0.234	1	0.234	11.45	<0.01
G_p	0.0423	1	0.0423	2.07	0.1541
$\mu_{s\ pp}$	56.74	1	56.74	2777.31	<0.01
$\mu_{r\ pp}$	57.88	1	57.88	2832.77	<0.01
$\mu_{s\ ps}$	13.6	1	13.6	665.8	<0.01
C_s	0.0721	1	0.0721	3.53	0.0641
$\mu_{r\ ps}$	15.07	1	15.07	737.6	<0.01
$v_p C_p$	0.0521	1	0.0521	2.55	0.1146
$v_p \mu_{r\ ps}$	0.0907	1	0.0907	4.44	0.0384
$G_p \mu_{s\ ps}$	0.0258	1	0.0258	1.26	0.2646
$G_p \mu_{r\ ps}$	0.0389	1	0.0389	1.90	0.1718
$\mu_{s\ pp}\ \mu_{r\ pp}$	0.0378	1	0.0378	1.85	0.1778
$\mu_{s\ pp}\ \mu_{s\ ps}$	0.0599	1	0.0599	2.93	0.0911
$\mu_{r\ pp} C_p$	0.0992	1	0.0992	4.85	0.0306
$\mu_{r\ pp} \mu_{s\ ps}$	0.0859	1	0.0859	4.2	0.0439
$\mu_{r\ pp} C_s$	0.0354	1	0.0354	1.73	0.1923
$C_p \mu_{r\ ps}$	0.0422	1	0.0422	2.06	0.1549
$\mu_{s\ pp}^2$	0.0846	1	0.0846	4.14	0.0454
C_p^2	0.0725	1	0.0725	3.55	0.0634
Residual	1.53	75	0.0204		
Lack of fit	1.45	68	0.0213	1.74	0.2258
Pure error	0.0855	7	0.0122		
R^2	0.9895				
Sum	146	119			

Table 6
The contribution rate of each factor to the simulated repose angle.

v_p	G_p	$\mu_{s\ pp}$	$\mu_{r\ pp}$	C_p	$\mu_{s\ ps}$	$\mu_{r\ ps}$	C_s
1.60	0.86	2.32	2.22	1.68	1.48	2.21	0.93

rolling friction ($\mu_{r\ pp}$), which further indicated that the effect of the coefficient of seed-to-seed rolling friction ($\mu_{r\ pp}$) was more pronounced for the angle of repose of the seeds.

3.6. Parameter optimization and simulation verification

Through the optimization module of Design-Expert 13.0 software, the second-order regression equation (5) was optimized and solved to obtain a set of the best simulation parameter combinations for pod pepper seeds by taking the actual repose angle as the target value (27.56°) to make the simulation test repose angle closest to the actual repose angle (27.56°): seed Poisson's ratio of 0.22, seed shear modulus of 15.47 MPa, seed-to-seed static friction coefficient of 0.25, seed-to-seed rolling friction coefficient of 0.67, seed-to-seed collision recovery coefficient of 0.64, seed-to-steel plate static friction coefficient of 0.55, seed-to-steel plate rolling friction coefficient of 0.45, and seed-to-steel plate collision recovery coefficient of 0.34.

Hou et al. stated that the physical angle of repose of ice grass seeds was not significantly different from the simulation test angle of repose by two-sample T test, and the relative error was small, which verified the authenticity of the simulation parameters [22]. Du et al. carried out the simulation verification test of the cylinder lifting method and pumping plate method, and the results manifested that the relative error between the simulated angle of repose of pod peppers and the physical angle of repose was within 3.35 %, which confirmed the credibility and reliability of the calibration parameters [41]. Chen et al. achieved the relative errors of the simulated angle of repose and the physical angle of repose obtained by the pumping plate method and the cylinder lifting method, respectively, to verify the accuracy of the calibration parameters [47]. Therefore, in this paper, the cylinder lifting method (as shown in Fig. 9(a)) and the pumping plate method (as shown in Fig. 9(b)) combined with the two-sample *t*-test were used to validate the reliability and authenticity of the discrete elemental parameters of the calibrated pod pepper seeds. By utilizing the parameters aforementioned as EDEM simulation parameters, a total of 10 simulation experiments were conducted. The angle of repose of pod pepper seeds was obtained as 26.43°, 28.36°, 27.18°, 29.27°, and 28.65° for the cylinder lifting method, and 25.83°, 27.36°, 28.48°, 29.77°, and 30.45° for the pumping plate method. Two-sample t-tests were performed on the simulated angle of repose and the physical test angle of repose for the two samples, respectively, resulting in $P_1 = 0.406 > 0.05$ and $P_2 = 0.493 > 0.05$ were obtained, indicating that there is no significant difference between the physical test angle of repose and the simulated test angle of repose after calibration of the simulation parameters. The average angle of repose of the particles acquired by the cylinder lifting method was 27.98°, with a relative

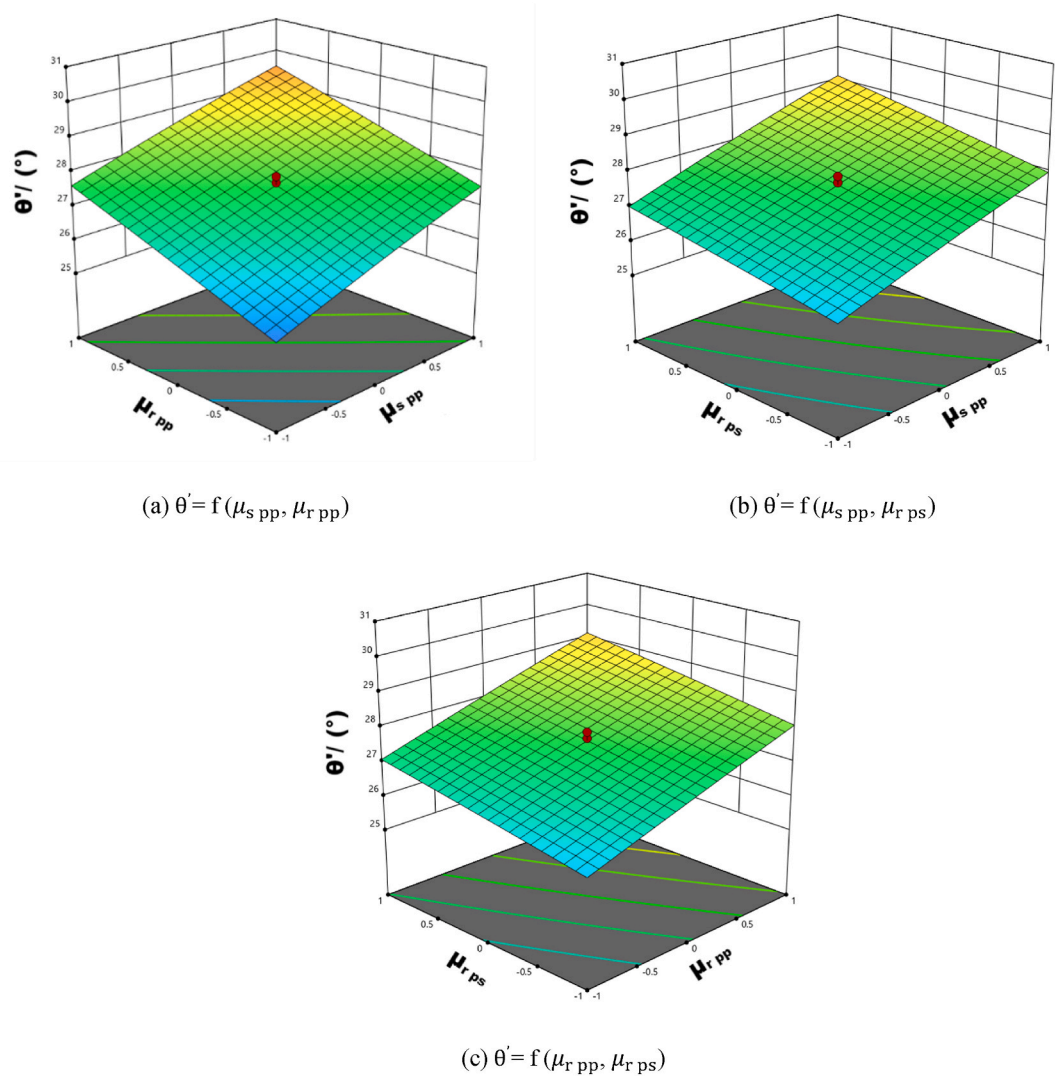

(a) $\theta' = f(\mu_{s\,pp}, \mu_{r\,pp})$ (b) $\theta' = f(\mu_{s\,pp}, \mu_{r\,ps})$

(c) $\theta' = f(\mu_{r\,pp}, \mu_{r\,ps})$

Fig. 8. Effect of factor interactions on angle of repose.

error of 1.524 % from the actual angle of repose of 27.56°. The average angle of repose of the particles realized by the pumping plate method was 28.38° with a relative error of 2.975 % to the actual angle of repose of 27.56°, which further proved the reliability and authenticity of the simulation test.

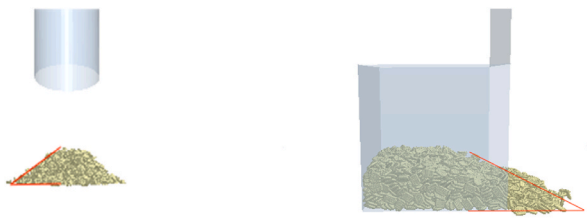

(a) (b)

Fig. 9. Verification test of calibration parameters (a) Cylinder lifting method (b) Pumping plate method.

4. Conclusions

(1) With the application of the reverse engineering technology, the shape contour of the pod pepper seeds was comprehensively scanned by the three-dimensional stereo laser scanner, which was encapsulated and then used to construct the seed particle simulation model by auto-filling in EDEM. A three-dimensional model group of the pod pepper seeds was established based on the distribution law of the measured pod pepper seeds' size ranges and frequencies in the process of discrete element simulation.

(2) The basic physical properties of pod pepper seeds were determined through physical tests combined with relevant literature at home and abroad, and the ranges of values of parameters such as external dimensions, density, water content, modulus of elasticity, shear modulus, Poisson's ratio, and so on, were identified for the seeds of pod pepper. Specifically, the values of static friction coefficient, rolling friction coefficient, and collision recovery coefficient between pod pepper seeds ranged from 0.20 to 0.60, 0.10–0.90, and 0.10–0.70, respectively; the values of static friction coefficient, rolling friction coefficient, and collision recovery coefficient between pod pepper seeds and steel plate were 0.20–0.60, 0.10–0.90, and 0.10–0.70, respectively; Poisson's ratio and shear modulus of pod pepper seeds ranged from 0.2 to 0.4 and 4–200 MPa, respectively.

(3) Box-Behnken central combination experimental design theory was chosen to conduct an eight-factor, three-level quadratic regression response surface test. Based on the test results, the quadratic regression model between each parameter and pod pepper seed rest angle was established and optimized. According to the analysis of variance (ANOVA), it was found that the primary and interaction terms of the five parameters, as well as the static friction coefficients of the pod pepper seeds and the quadratic terms of the seeds, imposed significant effects on the angle of repose of the pod pepper seeds. By analyzing the effect of each factor on the seed repose angle, the contribution of each factor to the simulated repose angle could be obtained, and the law of their action was explored by performing response surface analysis on the three factors with the largest contribution.

(4) The optimal simulation parameters were achieved by considering the measured pod pepper seed repose angle (27.56°) as the target value for the optimization of the solution, including: seed Poisson's ratio of 0.22, seed shear modulus of 15.47 MPa, seed-to-seed static friction coefficient of 0.25, seed-to-seed rolling friction coefficient of 0.67, seed-to-seed collision recovery coefficient of 0.64, seed-to-steel plate static friction coefficient of 0.55, seed-to-steel plate coefficient of rolling friction of 0.45, and seed-to-steel plate collision recovery coefficient of 0.34. Additionally, simulation validation tests were carried out for the cylinder lifting method and the pumping plate method, respectively, and the two-sample t-tests of the results of the two yielded $P_1 = 0.406 > 0.05$ and $P_2 = 0.493 > 0.05$, indicating that there was no significant difference in the angle of repose of pod pepper seeds obtained from the simulation test and the real test, and that the relative errors were 1.524 % and 2.975 %, respectively, which further verified the reliability and authenticity of the simulation. Overall, the reliability and authenticity of the test can be used as a reference for DEM calibration of other seeds with complex shapes.

Funding statement

This work was supported by the National Key Research and Development Project (No. 2022YFD2002403), Jiangsu Province Modern Agricultural Machinery Equipment and Technology Demonstration and Promotion Project (No. NJ2020-14), A Project Funded by the Priority Academic Program Development of Jiangsu Higher Education Institutions (NO. PAPD-2023-87).

CRediT authorship contribution statement

Xingye Chen: Writing – original draft, Software. **Xinzhong Wang:** Funding acquisition. **Jing Bai:** Writing – review & editing. **Weiquan Fang:** Formal analysis. **Tianyu Hong:** Data curation. **Nan Zang:** Validation. **Gaoliang Wang:** Investigation.

Declaration of competing interest

The authors declare no conflict of interest.

References

[1] J. Xu, X. Wang, S. Peng, C. Lian, Y. Ma, Z. Sun, L. Zhao, X. Liao, Monitoring natural drying process of chili peppers in Xinjiang Gobi Desert and developing its technical protocol, J. Chin. Inst. Food Sci. Technol. 23 (8) (2023) 274–285, https://doi.org/10.16429/j.1009-7848.2023.08.028.

[2] H. Xing, Z.M. Wang, X.W. Luo, S.Y. He, Y. Zang, Mechanism modeling and experimental analysis of seed throwing with rice pneumatic seed metering device with adjustable seeding rate, Comput. Electron. Agric. 178 (2020) 105697, https://doi.org/10.1016/j.compag.2020.105697.

[3] S. Mandal, G.V.P. Kumar, H. Tanna, A. Kumar, Design and evaluation of a pneumatic metering mechanism for power tiller operated precision planter, Curr. Sci. 115 (6) (2018) 1106–1114, https://doi.org/10.18520/cs/v115/i6/1106-1114.

[4] E.J. Ibrahim, Q.X. Liao, L. Wang, Y.T. Liao, L. Yao, Design and experiment of multi-row pneumatic precision metering device for rapeseed, Int. J. Agric. Biol. Eng. 11 (5) (2018) 116–123, https://doi.org/10.25165/j.ijabe.20181105.3544.

[5] W.Z. Zhang, C.L. Liu, Z.Q. Lu, X.T. Qi, H.Y. Lu, J.L. Hou, Optimized design and experiment on novel combination vacuum and spoon belt metering device for potato planters, Math. Probl Eng. 2020 (2020), https://doi.org/10.1155/2020/1504642. Article 1504642.

[6] B. Lenaerts, T. Aertsen, E. Tijskens, B. De Ketelaere, H. Ramon, J. De Baerdemaeker, W. Saeys, Simulation of grain-straw separation by Discrete Element Modeling with bendable straw particles, Comput. Electron. Agric. 101 (2014) 24–33, https://doi.org/10.1016/j.compag.2013.12.002.

[7] H. Kruggel-Emden, E. Simsek, S. Rickelt, S. Wirtz, V. Scherer, Review and extension of normal force models for the Discrete Element Method, Powder Technol. 171 (3) (2007) 157–173, https://doi.org/10.1016/j.powtec.2006.10.004.

[8] R. Shi, F. Dai, W. Zhao, F. Zhang, L. Shi, J. Guo, Establishment of discrete element flexible model and verification of contact parameters of flax stem, Nongye Jixie Xuebao/Transactions of the Chinese Society for Agricultural Machinery 53 (10) (2022) 146–155, https://doi.org/10.6041/j.issn.1000-1298.2022.10.015.

[9] J. Guo, M. Karkee, Z. Yang, H. Fu, J. Li, Y.L. Jiang, T.T. Jiang, E.X. Liu, J.L. Duan, Discrete element modeling and physical experiment research on the biomechanical properties of banana bunch stalk for postharvest machine development, Comput. Electron. Agric. 188 (2021), https://doi.org/10.1016/j.compag.2021.106308. Article 106308.

[10] F. Peng, H. Wang, F. Fang, Y. Liu, Calibration of discrete element model parameters for pellet feed based on injected section method, Nongye Jixie Xuebao/Transactions of the Chinese Society for Agricultural Machinery 49 (4) (2018) 140–147, https://doi.org/10.6041/j.issn.1000-1298.2018.04.016.

[11] R. Zhang, W. Jiao, J. Zhou, B. Qi, H. Liu, Q. Xia, Parameter calibration and experiment of rice seeds discrete element model with different filling particle radius, Nongye Jixie Xuebao/Transactions of the Chinese Society for Agricultural Machinery 51 (2020) 227–235, https://doi.org/10.6041/j.issn.1000-1298.2020.S1.026.

[12] C.J. Coetzee, D.N.J. Els, G.F. Dymond, Discrete element parameter calibration and the modelling of dragline bucket filling, J. Terramechanics 47 (1) (2010) 33–44, https://doi.org/10.1016/j.jterra.2009.03.003.

[13] S. Lee, J. Park, Standardized friction experiment for parameter determination of discrete element method and its validation using angle of repose and hopper discharge, Multiscale Science and Engineering 1 (2019) 247–255.

[14] B.M. Ghodki, M. Patel, R. Namdeo, G. Carpenter, Calibration of discrete element model parameters: soybeans, Computational Particle Mechanics 6 (1) (2019) 3–10, https://doi.org/10.1007/s40571-018-0194-7.

[15] Y. Wang, Z. Liang, D. Zhang, T. Cui, S. Shi, K. Li, L. Yang, Calibration method of contact characteristic parameters for corn seeds based on EDEM, Nongye Gongcheng Xuebao/Transactions of the Chinese Society of Agricultural Engineering 32 (22) (2016) 36–42, https://doi.org/10.11975/j.issn.1002-6819.2016.22.005.

[16] W. Liu, J. He, H. Li, X. Li, K. Zheng, Z. Wei, Calibration of simulation parameters for potato minituber based on EDEM, Nongye Jixie Xuebao/Transactions of the Chinese Society for Agricultural Machinery 49 (5) (2018) 125–135, https://doi.org/10.6041/j.issn.1000-1298.2018.05.014.

[17] S. Zhang, R. Zhang, T. Chen, J. Fu, H. Yuan, Calibration of simulation parameters of mung bean seeds using discrete element method and verification of seed-metering test, Nongye Jixie Xuebao/Transactions of the Chinese Society for Agricultural Machinery 53 (3) (2022) 71–79, https://doi.org/10.6041/j.issn.1000-1298.2022.03.007.

[18] R. Zhang, D.L. Han, Q.L. Ji, Y. He, J.Q. Li, Calibration methods of sandy soil parameters in simulation of discrete element method, Trans. Chin. Soc. Agric. Mach. 48 (3) (2017) 49–56, https://doi.org/10.6041/j.issn.1000-1298.2017.03.006.

[19] J. Wang, Y. Zhang, R. Gu, Research status and prospects on plant canopy structure measurement using visual sensors based on three-dimensional reconstruction, Agriculture-Basel 10 (46210) (2020), https://doi.org/10.3390/agriculture10100462.

[20] J.M. Boac, M.E. Casada, R.G. Maghirang, J.P. Harner III, Material and interaction properties of selected grains and oilseeds for modeling discrete particles. Trans, ASABE (Am. Soc. Agric. Biol. Eng.) 53 (2010) 1201–1216, https://doi.org/10.13031/2013.32577.

[21] L. Shi, Z. Ma, W. Zhao, X. Yang, B. Sun, J. Zhang, Calibration of simulation parameters of flaxed seeds using discrete element method and verification of seed-metering test, Nongye Gongcheng Xuebao/Transactions of the Chinese Society of Agricultural Engineering 35 (20) (2019) 25–33, https://doi.org/10.11975/j.issn.1002-6819.2019.20.004.

[22] Z. Hou, N. Dai, Z. Chen, Y. Qiu, X. Zhang, Measurement and calibration of physical property parameters for Agropyron seeds in a discrete element simulation, Nongye Gongcheng Xuebao/Transactions of the Chinese Society of Agricultural Engineering 36 (24) (2020) 46–54, https://doi.org/10.11975/j.issn.1002-6819.2020.24.006.

[23] J. Hao, W. Wei, P. Huang, J. Qin, J. Zhao, Calibration and experimental verification of discrete element parameters of oil sunflower seeds, Nongye Gongcheng Xuebao/Transactions of the Chinese Society of Agricultural Engineering 37 (12) (2021) 36–44, https://doi.org/10.11975/j.issn.1002-6819.2021.12.005.

[24] F. Liu, J. Zhang, B. Li, J. Chen, Calibration of parameters of wheat required in discrete element method simulation based on repose angle of particle heap, Nongye Gongcheng Xuebao/Transactions of the Chinese Society of Agricultural Engineering 32 (12) (2016) 247–253, https://doi.org/10.11975/j.issn.1002-6819.2016.12.035.

[25] F. Jia, L. Yao, Y. Han, H. Wang, Y. Shi, Y. Zeng, L. Jiang, Simulation and optimal design of uniform plate of brown rice based on discrete element method, Nongye Gongcheng Xuebao/Transactions of the Chinese Society of Agricultural Engineering 32 (4) (2016) 235–241, https://doi.org/10.11975/j.issn.1002-6819.2016.04.033.

[26] J. Horabik, M. Molenda, Parameters and contact models for DEM simulations of agricultural granular materials: a review, Biosyst. Eng. 147 (2016) 206–225, https://doi.org/10.1016/j.biosystemseng.2016.02.017.

[27] D. Markauskas, Á. Ramírez-Gómez, R. Kačianauskas, E. Zdancevičius, Maize grain shape approaches for DEM modelling, Comput. Electron. Agric. 118 (2015) 247–258, https://doi.org/10.1016/j.compag.2015.09.004.

[28] J. Wiacek, M. Molenda, J. Horabik, J.Y. Ooi, Influence of grain shape and intergranular friction on material behavior in uniaxial compression: experimental and DEM modeling, Powder Technol. 217 (2012) 435–442, https://doi.org/10.1016/j.powtec.2011.10.060.

[29] Y. Wang, J. He, H. Yang, Y. Guo, J. Lu, Simulation parameter calibration of broad bean seed discrete element model[J], Agric. Eng. 13 (1) (2023), 79-84 . DOI : 10.19998/j.cnki.2095-1795.2023.01.015.

[30] N. Dai, Z. Hou, Y. Chou, X. Zhang, Calibration and experiment of discrete element simulation parameters of red clover seeds, Journal of hebei agricultural university.06 (2021) 92–98, https://doi.org/10.13320/j.cnki.jauh.2021.0107.

[31] H. Sun, S. Li, X. Hang, J. Wu, F. Wan, Discrete element model construction and seed flesh separation process of seed gourd, Journal of Northwest Agriculture and Forestry University (Natural Science Edition) (10) (2022) 144–154, https://doi.org/10.13207/j.cnki.jnwafu.2022.10.015.

[32] J. Wu, C. Cao, C. Xie, L. Fang, Z. Wu, M. Hu, T. Wang, Measurement of physical parameters of Radix peucedani seeds and parameter calibration of discrete element simulation model, Journal of Gansu Agricultural University (4) (2019) 180–189, https://doi.org/10.13432/j.cnki.jgsau.2019.04.024.

[33] C.M. Wensrich, A. Katterfeld, Rolling friction as a technique for modelling particle shape in DEM, Powder Technol. 217 (2012) 409–417, https://doi.org/10.1016/j.powtec.2011.10.057.

[34] Z. Xu, S. Wang, Z. Yi, J. P, X. Lu, Parameter calibration of chili seed discrete element based on JKR model, Journal of Chinese Agricultural Mechanization 44 (9) (2023) 85–95, https://doi.org/10.13733/j.jcam.issn.2095-5553.2023.09.013.

[35] X. Huang, X. Zha, H. Pan, W. Zong, H. Chen, Measurement and analysis of rapeseeds' restitution coefficient in point-to-plate collision model, Trans. Chin. Soc. Agric. Eng. 30 (24) (2014) 22–29.

[36] X. Cheng, H. Li, C. Lu, J. He, Q. Wang, C. Wang, C. Yu, Z. Wei, C. Wang, Parameter optimization and experiment of centrifugal seed dispenser in wheat plot drill, Trans. Chin. Soc. Agric. Eng. 35 (20) (2019) 1–9, https://doi.org/10.11975/j.issn.1002-6819.2019.20.001.

[37] Y. Wang, F.Y. Lu, T.Y. Xu, J.Q. Yu, Shape and size analysis of soybean kernel and modeling, Jilin Daxue Xuebao (Gongxueban)/Journal of Jilin University (Engineering and Technology Edition) 48 (2018) 507–517, https://doi.org/10.13229/j.cnki.jdxbgxb20170953.

[38] C.K. Kanakabandi, T.K. Goswami, Determination of properties of black pepper to use in discrete element modeling, J. Food Eng. 246 (2019) 111–118, https://doi.org/10.1016/j.jfoodeng.2018.11.005.

[39] M. Wu, J. Cong, Q. Yan, T. Zhu, X. Peng, Y. Wang, Calibration and experiments for discrete element simulation parameters of peanut seed particles, Nongye Gongcheng Xuebao/Transactions of the Chinese Society of Agricultural Engineering 36 (23) (2020) 30–38, https://doi.org/10.11975/j.issn.1002-6819.2020.23.004.

[40] Q. Yang, L. Shi, A. Shi, M. He, X. Zhao, L. Zhang, M. Addy, Determination of key soil characteristic parameters using angle of repose and direct shear stress test, Int. J. Agric. Biol. Eng. 16 (3) (2023) 143–150, https://doi.org/10.25165/j.ijabe.20231603.6293.

[41] C.X. Du, D.L. Han, Z.Q. Song, Y.C. Chen, X.G. Chen, X.Z. Wang, Calibration of contact parameters for complex shaped fruits based on discrete element method: the case of pod pepper (Capsicum annuum), Biosyst. Eng. 226 (2023) 43–54, https://doi.org/10.1016/j.biosystemseng.2022.12.005.

[42] R. Yue, J. Hu, Y. Liu, M. Yao, T. Zhang, J. Shi, Design and working parameter optimization of pneumatic reciprocating seedling-picking device of automatic transplanter, Agriculture-Basel 12 (2022) 198912, https://doi.org/10.3390/agriculture12121989.

[43] W. Wang, X. Lv, Z. Yi, Parameter optimization of reciprocating cutter for Chinese little greens based on finite element simulation and experiment, Agriculture-Basel 12 (2022) 213112, https://doi.org/10.3390/agriculture12122131.

[44] W.Q. Fang, X.Z. Wang, D.L. Han, X.G. Chen, Review of material parameter calibration method, Agriculture-Basel 12 (5) (2022), https://doi.org/10.3390/agriculture12050706. Article 706.
[45] H. Yuan, S. Liang, J. Wang, Y. Lu, Numerical simulation and analysis of vibrating rice filling based on EDEM software, Agriculture-Basel 12 (2022) 201312, https://doi.org/10.3390/agriculture12122013.
[46] Z. Ma, Advanced Biostatistics [M], Science Press, Beijing, 2016.
[47] Y. Chen, X. Gao, X. Jin, X. Ma, B. Hu, X. Zhang, Calibration and Analysis of Seeding Parameters of Cyperus Esculentus Seeds Based on Discrete Element Simulation, Nongye Jixie Xuebao/Transactions of the Chinese Society for Agricultural Machinery, 2023, pp. 1–14. https://link.cnki.net/urlid/11.1964.S.20231011.1816.008.